JOURNAL OF MATERIALS SCIENCE 30 (1995) 53–62

Pyrosol deposition of fluorine-doped tin dioxide thin films

J. DUTTA**, J. PERRIN, T. EMERAUD
Laboratoire de Physique des Interfaces et des Couches Minces, CNRS UPR AO258, Ecole Polytechnique, 91128 Palaiseau cédex, France, and Solems S. A., 3 rue Léon Blum, Z.I. Les Glaises, 92124 Palaiseau cédex, France

J.-M. LAURENT, A. SMITH*
Laboratoire de Matériaux Céramiques et de Traitement des Surfaces, CNRS URA 320, Ecole Nationale Supérieure de Céramique Industrielle, 47 à 73, Avenue Albert Thomas, 87065 LIMOGES cédex, France

Fluorine-doped tin dioxide (SnO_2:F) films were deposited from a tin tetrachloride solution in methanol utilizing a pyrosol deposition process. It is shown from thermodynamic calculations that the atmosphere during deposition is oxygen-rich and also suggested that chlorine and hydrogen chloride, which are produced during the deposition reaction, influence crystal growth. Detailed electrical, optical and structural properties of the material with respect to varying film thickness and substrate temperature are presented and discussed. Resistivity of the films deposited at 450 °C decreased from 6×10^{-4} to $2 \times 10^{-4}\,\Omega$ cm, while the mobility increased from 14 to 45 $cm^2 V^{-1} s^{-1}$, respectively, when the film thickness was varied from 100 to 1650 nm. The carrier concentration was relatively unchanged for film thicknesses higher than 200 nm. Optimized SnO_2:F films ($\sim$600 nm) having a resistivity of $\sim 6 \times 10^{-4}\,\Omega$ cm, a carrier mobility of $\sim 20\,cm^2 V^{-1} s^{-1}$, a carrier concentration of $\sim 8 \times 10^{20}\,cm^{-3}$ and a transmittance in excess of 80% are quite suitable as electrodes for amorphous silicon solar cells.

1. Introduction

Transparent conducting oxide (TCO) thin films have found a wide range of applications especially in opto-electronic devices, photovoltaic devices, sensors, etc. Thin layers of non-stoichiometric metal oxides like tin oxide, indium oxide, cadmium oxide, zinc oxide and their alloys when deposited under appropriate conditions are optically transparent as well as electrically conducting [1]. Ever since the first successful implementation of the spray pyrolysis deposition process [2] for the commercial production of tin dioxide coated glass substrates, several techniques have been developed for TCO deposition. Depending on the nature of its application, an appropriate deposition process is chosen for the growth of TCO films. TCO coatings on glass have been traditionally grown either by spray pyrolysis or by "atmospheric pressure chemical vapour deposition" (APCVD) processes [1]. Often spray pyrolysis is preferred to chemical vapour deposition (CVD) because of the relative simplicity in the control of the process parameters.

In the spray pyrolysis process, an inorganic, or organometallic precursor is dissolved in a solvent which is then sprayed on a heated substrate where the constituents react to form a chemical compound. The reactants are chosen such that the products other than those desired are volatile at the deposition temperature. The essential difference between spray pyrolysis and the pyrosol technique is that in the former case a carrier gas is saturated with the reactant solution which is then transported onto the substrates by injection through a sprayer under adequate gas pressure. In the pyrosol process, however, the reactant is nebulized by ultrasonic excitation and the resultant aerosol is then carried by a gas onto the heated substrate. Much better control of the droplet size and distribution can be achieved and hence control of process parameters becomes easier when using the pyrosol deposition technique [3–6].

Fluorine-doped tin dioxide (SnO_2:F) thin films have attracted a lot of attention in recent times especially because of their application as an electrode of amorphous silicon (a-Si) solar cells [4, 5, 7, 8]. SnO_2:F films have improved opto-electronic properties compared with undoped tin dioxide films and are also more resistant to chemical attack [1, 9, 10]. There

*All correspondence to Dr Agnès Smith.
** *Present address*: Ecole Polytechnique Féderale de Lausanne, Laboratoire de Technologie des Poudres, MX-D Ecublens, CH-1015 Lausanne.

0022–2461

are several commercial manufacturers producing special coatings of SnO_2:F films on glass for application in a-Si solar cells. In a previous paper we reported the implementation of the pyrosol deposition process for large area uniform deposition of SnO_2:F thin films [11]. Here we examine the chemical nature and quantities of species produced during the deposition process based on a thermodynamical approach. These results are correlated with the film morphology and the variation of film properties with the film thickness and the deposition temperature is also addressed.

2. Experimental details

All the depositions were done on alumina-coated soda lime glass substrates (80 cm long × 10 cm wide × 0.2 cm thick). Alumina coating on the glass (deposited at 520 °C) was essential as a diffusion barrier to prevent contamination of SnO_2:F layers by Na^+, K^+ or Ca^{++} from the glass substrate. The SnO_2:F deposition was carried out from a starting solution of tin tetrachloride, $SnCl_4$ (0.4 $moll^{-1}$) in methanol (CH_3OH). Ammonium fluoride (NH_4F) was added to this mixture for fluorine doping. The F/Sn atomic ratio in the starting solution was kept constant (5%) for all the depositions reported here. The deposition set-up, which is shown in Fig. 1, essentially consists of a pyrosol generator and a pyrolysis region. The pyrosol generator includes a pot containing the reactant which is separated from a piezoelectric transducer through a thin non-permeable membrane. The energy dissipated by the piezoelectric transducer which is immersed in deionized water is transferred, through the membrane, to the reactant liquid which is to be nebulized. Such a design is necessary to avoid any possible damage of the transducer by the reactant solution (such as corrosion of the metallic electrodes etc.). Details of the pyrosol generator and the fundamental processes governing the aerosol generation are given elsewhere [11]. The pyrosol generator is coupled to a level controller which works on the principle of a manometer in order to maintain a constant volume of reactant liquid in the pot to achieve constant-volume averaged energy dissipation at all times. The nebulized liquid was carried by a flow (200 lh^{-1}) of nitrogen gas into the furnace. A separate port in the furnace was used to feed additional air (800 lh^{-1}) in the deposition zone to proceed with the reaction of the precursors. The glass substrate is mounted on a perforated plate which is enclosed in a metal shield as shown in Fig. 1. Heating is carried out from both sides of the furnace using resistive elements. An exhaust is drawn out from the other end of the furnace and the unreacted gases are passed through activated charcoal before being removed through the exhaust duct. The samples were loaded from the exhaust side of the furnace and left to thermalize for 30 min prior to each deposition.

To keep the nebulized liquid flow constant, which is necessary for a stable and reproducible deposition process, it is very important to monitor the variation in the mass flow from the pyrosol pot with respect to time. In fact, we observed previously that it takes about 40 min for the system to stabilize [11]. In order to obtain maximum transfer of energy to the reactant liquid in our configuration, the excitation frequency

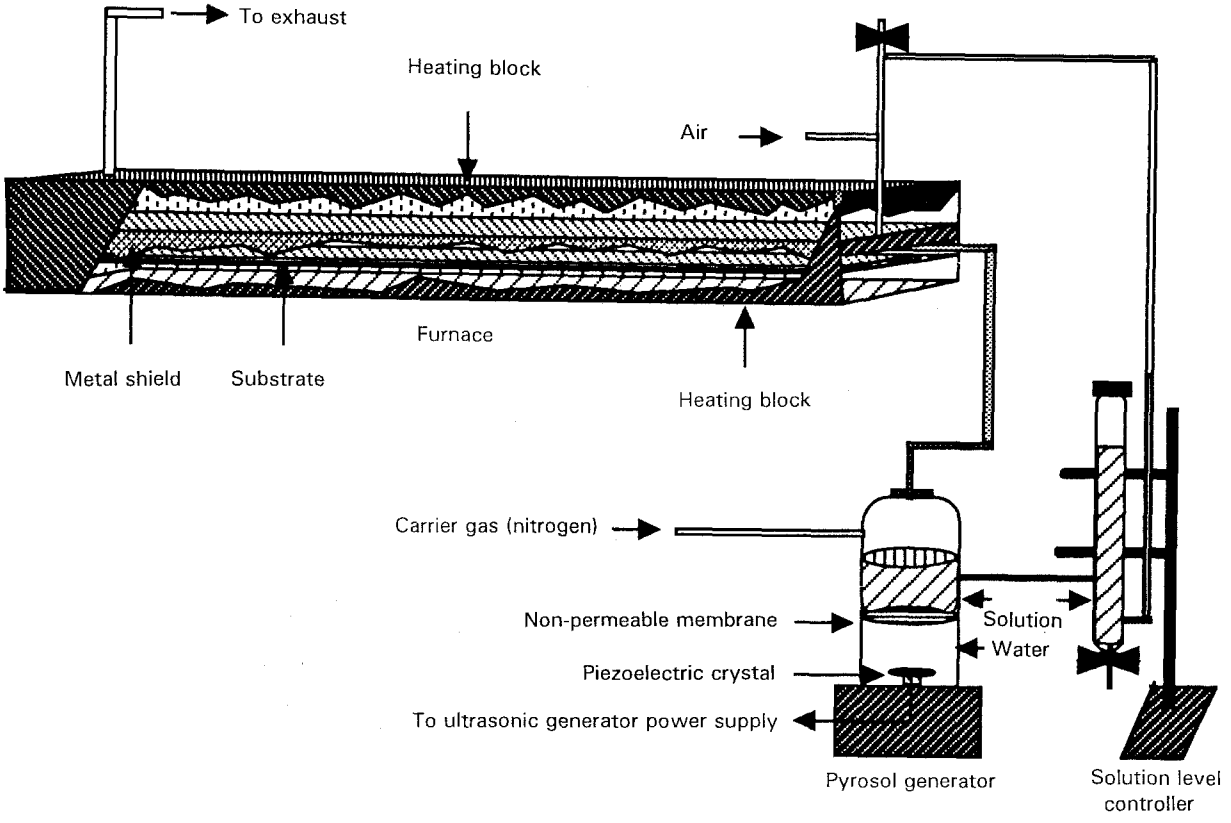

Figure 1 A deposition set-up.

was optimized. Fig. 2 shows the changes in mass flow of the nebulized liquid with varying frequency of excitation at 40% power (total power of the source was 200 W). The mass flow measurement was carried out in a system as described elsewhere [11]. All depositions were carried out after allowing the operating frequency to settle down, with 40% power at 900 kHz frequency where the mass flow is highest. The higher aerosol generation directly results in increased growth rates as shown in Fig. 3.

Since a large volume of dynamic gas flow is involved in the deposition process ($1000\,l\,h^{-1}$) it is always necessary to determine the temperature in the vicinity of the substrate surface under gas flow. In Fig. 4a the temperature profile on a glass substrate (furnace temperature 500 °C) with and without gas flow is shown and was determined by placing copper-constantan thermocouples at every 5 cm of the substrate (Fig. 4b). It can be seen that the temperature profile is rather flat around 30–40 cm from the edge of the glass plate near the inlet of the aerosol flow. Knowing the exact temperature drop in this region we made appropriate corrections to the temperature measurements carried out with the thermocouple fitted on to the furnace to determine the substrate temperature during deposition.

Small pieces (1.5 × 1.5 cm) of the samples were cut from the glass substrate, 35 cm from the edge of the substrate where the aerosol was injected (Fig. 4b). Thickness was determined using a Sloan-Dektak II step profiler after etching a step on the coating with hydrochloric acid in the presence of zinc powder. All the electrical, optical and structural characterizations were done at room temperature. The infrared (IR) spectra were also recorded at room temperature in a Perkin-Elmer 1750 Fourier transform spectrophotometer using KBr windows. The resistivity, carrier mobility and carrier concentration were determined by measurement of Hall resistivity in a maximum magnetic field of 8.4 kG by the Van der Pauw technique. Square configuration of the samples was chosen to avoid contact placement errors as pointed out by Koon *et al.* [12]. The optical transmittance of TCO films on glass substrates was measured in the 400–1100 nm wavelength range using a ROFIN-

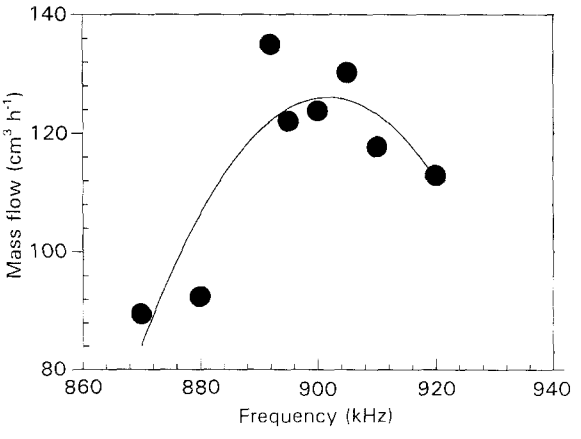

Figure 2 Mass flow of methanol as a function of aerosol generator frequency.

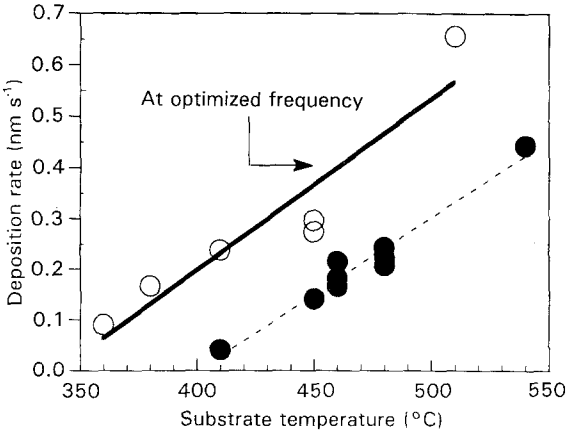

Figure 3 Deposition rate versus temperature for different frequencies (● 750 kHz; ○ 900 kHz).

SINAR fast spectrophotometer (RSO 6240). In air, total transmittance consists of specular and diffuse components due to the TCO roughness. The specular transmittance of the as-deposited sample was measured in air. Moreover, in order to obtain an equivalent of the total transmittance, the sample was covered by a low absorbing liquid having a refractive index $n = 1.78$, approximately matching the TCO refractive index, which reduces light scattering from rough surfaces. This type of measurement gives a reasonable estimate of the total transmission of the rough TCO films as has been evidenced by earlier measurements and theoretical models [13]. Hereafter, this measurement is referred to as matching liquid transmittance (MLT). The transmission spectra was integrated over the 400–1100 nm range. Scanning electron microscopy (SEM) was done using a Hitachi 2000 electron microscope with an acceleration voltage of 30 kV.

3. Results and discussion

3.1. Chemical species during film formation

The pyrosol process can be described as a two-stage process. First there is the production of the precursors in the aerosol followed by the CVD of the reactants. In order to identify the chemical nature of species responsible for the deposition, we carried out a distillation experiment with a solution of tin tetrachloride ($0.4\,mol\,l^{-1}$) dissolved in methanol. All the glass parts (container, distillation column, condensation coil, collecting flask), were carefully dried before mounting. The whole glass assembly was demoisturized prior to the experiment. These precautions were necessary to avoid any unwanted hydrolysis of tin tetrachloride [14]. The starting solution boiled at 65 °C and the temperature at the top of the distillation column was also 65 °C (stage I). This suggests that the evaporated gas remains at the solution temperature. Stage I corresponds to the distillation of methanol since its boiling point is 65 °C [15]. Once the alcohol was mostly distilled off, the temperature of the solution increased to about 100 °C (stage II) at which point some solid condensation took place on the glass container. As the experiment continued, the temperature in the flask went up to 114 °C (stage III) and the

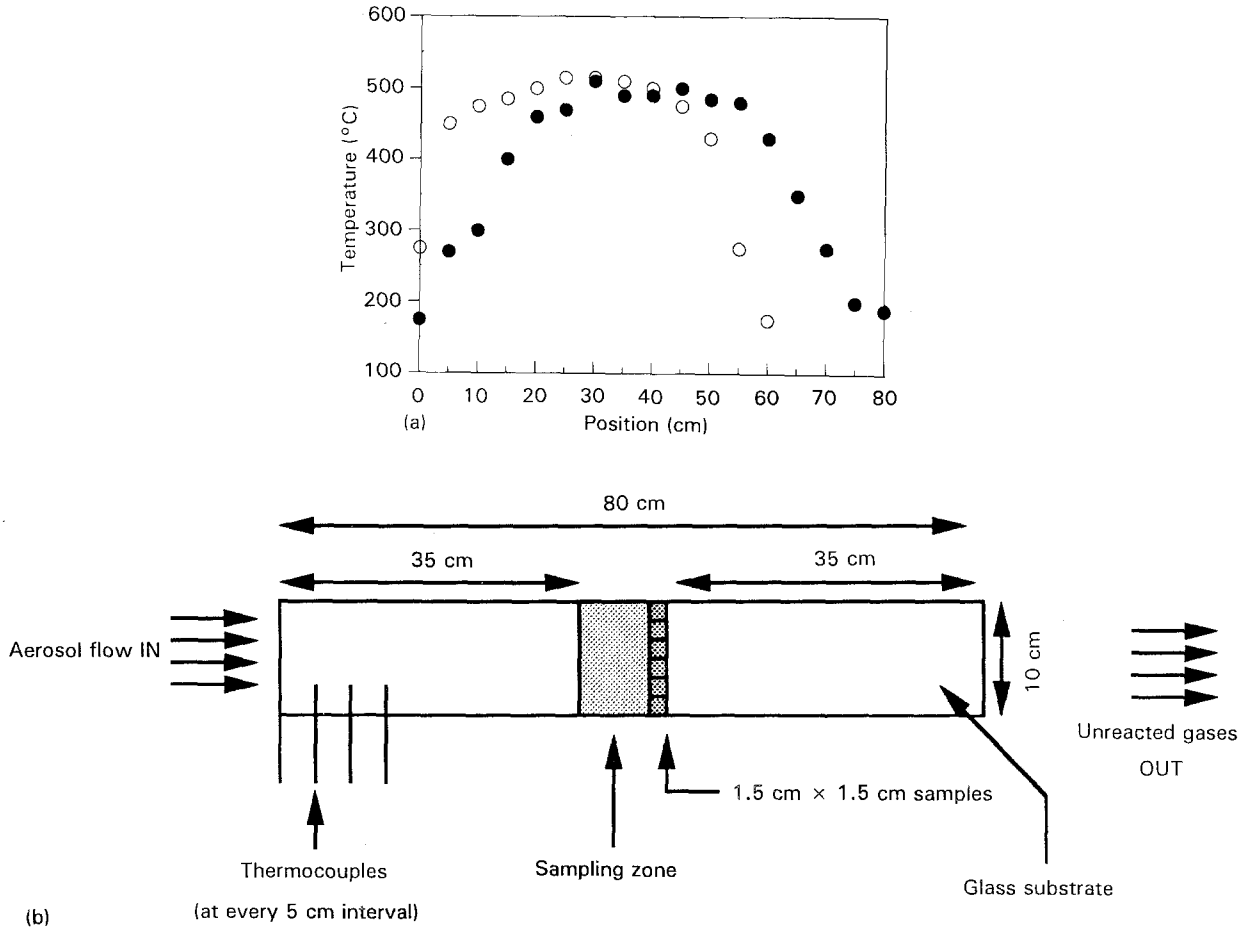

Figure 4 (a) Temperature profile on the glass plate with and without gas flow; (b) description of experimental set-up for measuring the temperature on the glass plate. ○, T (°C): no gas; ●, T (°C): with gas flow.

previously condensed solid redissolved in the hot vapour. When ammonium fluoride (F/Sn = 5 at%) was added in the solution of tin tetrachloride (0.4 $moll^{-1}$) dissolved in methanol we did not notice any modification of the distillation stages previously described.

Before interpreting the phenomena occurring at 100 and 114 °C, let us first examine the chemical nature of species in the starting solution. In the absence of moisture, $SnCl_4$, which is a strong Lewis acid, forms colourless complexes with methanol, mostly of the type $SnCl_4.2CH_3OH$ [14]. Each molecule of the complex is surrounded by solvent molecules forming a cluster. As the distillation proceeds in stage I, the ratio of $n(CH_3OH)/n(SnCl_4 \cdot 2CH_3OH)$ decreases, where $n(CH_3OH)$ and $n(SnCl_4 \cdot 2CH_3OH)$ correspond to the molar concentrations of solvent and tin (IV) complexes respectively. The condensed solid at stage II is obviously $SnCl_4 \cdot 2CH_3OH$ because it has been reported that its melting point ranges between 99 and 106 °C [14]. An IR spectrum of the distillation residue in the flask at this stage of the experiment (Fig. 5) shows that the C–O vibration at 970 cm^{-1} corresponds to a shift by about 50 cm^{-1} below its value in CH_3OH, which is characteristic of $SnCl_4 \cdot 2CH_3OH$ complexes. Stage III correlates with the boiling point of $SnCl_4$ [16]. As the temperature goes up and the reaction proceeds (stage II to stage III), $SnCl_4 \cdot 2CH_3OH$ complexes transform into $SnCl_4$ according

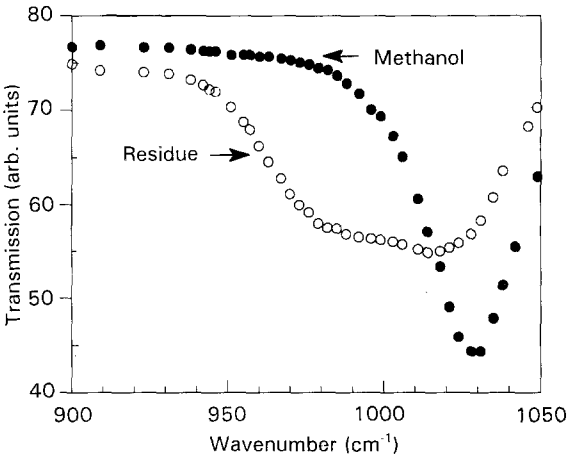

Figure 5 IR spectra for methanol and distillation residue which formed at 100 °C.

to the following reaction:

$$SnCl_4 \cdot 2CH_3OH \Rightarrow SnCl_4 + 2CH_3OH \quad (1)$$

This simple distillation experiment signifies that the chemical species contained in the droplets which arrive in the pyrolysis region are the solvent, CH_3OH, and tin in the form of a complex $SnCl_4 \cdot 2CH_3OH$. The gaseous molecules, like oxygen and nitrogen, are brought in by the carrier gas. The CVD of the reactants in the pyrolysis region corresponds to several

simultaneous reactions. First of all, the solvent is decomposed through a combustion reaction:

$$CH_3OH + 3/2O_2 \Rightarrow CO_2 + 2H_2O \quad (2)$$

With calculations based on the minimization of the Gibbs free enthalpy of the system, and mass conservation equations for all the elements, it is possible to calculate the quantities of gaseous species resulting from the pyrolysis of precursors available for the final deposition process [17, 18]. This approach, which is frequently used to describe the CVD processes, gives interesting insight into the chemical nature of the gaseous species which take part in the deposition. In our case, since the volume of nebulized solution was about 2 $cm^3 min^{-1}$ (Fig. 2) and the gas flows were, respectively, 3.3 $l min^{-1}$ and 13.3 $l min^{-1}$, for nitrogen and air: the starting quantities of the constituents were 49.3×10^{-3} mol min^{-1} for CH_3OH, 8×10^{-4} mol min^{-1} for $SnCl_4$, 4×10^{-5} mol min^{-1} for NH_4F, 0.125 mol min^{-1} for O_2 and 0.619 mol min^{-1} for N_2. The calculations show that in the temperature range of our interest (360–500 °C), methanol is completely burnt out and the surrounding atmosphere is oxidizing. Apart from solid SnO_2, oxygen is in the form of O_2, H_2O and CO_2. The quantities of O_2, H_2O and CO_2 are, respectively, equal to 0.051, 98.6×10^{-3} and 49.3×10^{-3} mol min^{-1}. H_2O and CO_2 result from the decomposition of CH_3OH, while the oxygen quantity represents what is left after the combustion reaction 2. Concerning tin, the complex undergoes reaction 1. Since $SnCl_4$ is produced, it converts into SnO_2 [19], either by reaction with the ambient oxygen or with the water produced through reaction 2:

$$SnCl_4 + O_2 \Rightarrow SnO_2 + 2Cl_2 \quad (3)$$

$$SnCl_4 + 2H_2O \Rightarrow SnO_2 + 4HCl \quad (4)$$

The quantities of both O_2 and H_2O reacting with $SnCl_4$ to form SnO_2, as described by Ghostagore [19], are small compared with the available amounts. The calculations based on the approach used by White *et al.* [17, 18] for our situation show that the amount of HCl produced by reaction 4 is constant between 360 and 500 °C and is equal to 3×10^{-3} mol min^{-1}, while the amount of Cl_2, produced by reaction 3, decreases linearly with increasing temperatures from 1.11×10^{-4} mol min^{-1} (at 360 °C) to 1.42×10^{-5} mol min^{-1} (at 500 °C). Reactions 3 and 4 lead to the production of highly chlorinated gases which can etch the growing SnO_2 layer [20, 21]. At this point in the discussion it is emphasized that the gaseous species can either be in the boundary layer close to the substrate, or on the solid surface itself.

3.2. Variation of morphology

3.2.1. Effect of thickness

In order to study the growth of the crystallites and its influence on the film properties, films of different thicknesses were deposited under identical conditions. Films were deposited at 450 °C for various deposition times to obtain samples of thicknesses varying from 100 to 1650 nm. Earlier we observed that films thinner than 100 nm are not well crystallized [11] and hence we did not attempt to include the properties of films thinner than 100 nm in this study. Fig. 6a–g are micrographs of some of our SnO_2:F films of different thicknesses varying from 100 to 1650 nm and deposited at 450 °C. Films less than 350 nm thick were very heterogeneous with noticeable voids (Fig. 6a–c). Such voids can originate from a non-uniform nucleation at the Al_2O_3 surface arising from thermal relaxation processes. Similar heterogeneous deposition has been observed in the case of thin metal films [22]. Beyond a thickness of 350 nm, the films were very homogeneous (practically no voids (Fig. 6d–g)) and were well crystallized. The crystal sizes in typical 100 nm thick films were around 50–200 nm, while for the 1650 nm thick film the crystal sizes varied between 150 and 750 nm. The crystal size and the size distribution of crystallites in the films between 350 and 650 nm thick were fairly similar, with the maximum and minimum sizes between 350 and 50 nm respectively. It is thus not surprising that most of the results reported in the literature as optimized TCO films are for 400–650 nm thick films [1].

3.2.2. Effect of substrate temperature

SnO_2:F films were deposited at different substrate temperatures and Fig. 7a–e are micrographs of samples deposited at 360, 380, 410, 450 and 510 °C, respectively. The films have an amorphous texture when deposited at lower temperatures (< 410 °C) but crystals begin to form at deposition temperatures around 410 °C and higher. The crystal size is not uniform and generally many different crystal sizes (50–250 nm) could be observed in such films. Also the smallest and largest crystallites were equally distributed (Fig. 7c). For the films deposited at 450 °C, the number of large crystallites increased rapidly as also did crystallite size, which varied from 80 to 400 nm (Fig. 7d). On further increase of the substrate temperature (510 °C in our case) the distribution of small and large crystallites is about the same except that some large crystallites of 500 nm could also be observed (Fig. 7e). The effect of substrate temperature can be interpreted as follows [23]: at $T < 410$ °C, the deposition process is led by nucleation and the fine-grained morphologies result in the deposit which is amorphous in the absence of any crystal growth. The excess surface-free energy of the deposited nuclei provokes coalescence phenomena leading to the well known "spherulites" or "cauliflowers". In the present case the resulting morphology is smooth. Cl_2, which is particularly known as an etchant, and HCl for coarsening of oxides during their sintering, may lead to the smoother surfaces at lower temperatures [20, 21]. As the temperature increases, the combined effects of a decrease in Cl_2 concentration compared with the available HCl (as seen from our calculations) and the crystal growth, lead to a rougher surface. Such variations in the process could also lead to the differences in grain sizes observed on films deposited above 450 °C. Again, the deposition rate increases with the substrate temperature from 0.092 nm s^{-1} at 360 °C to

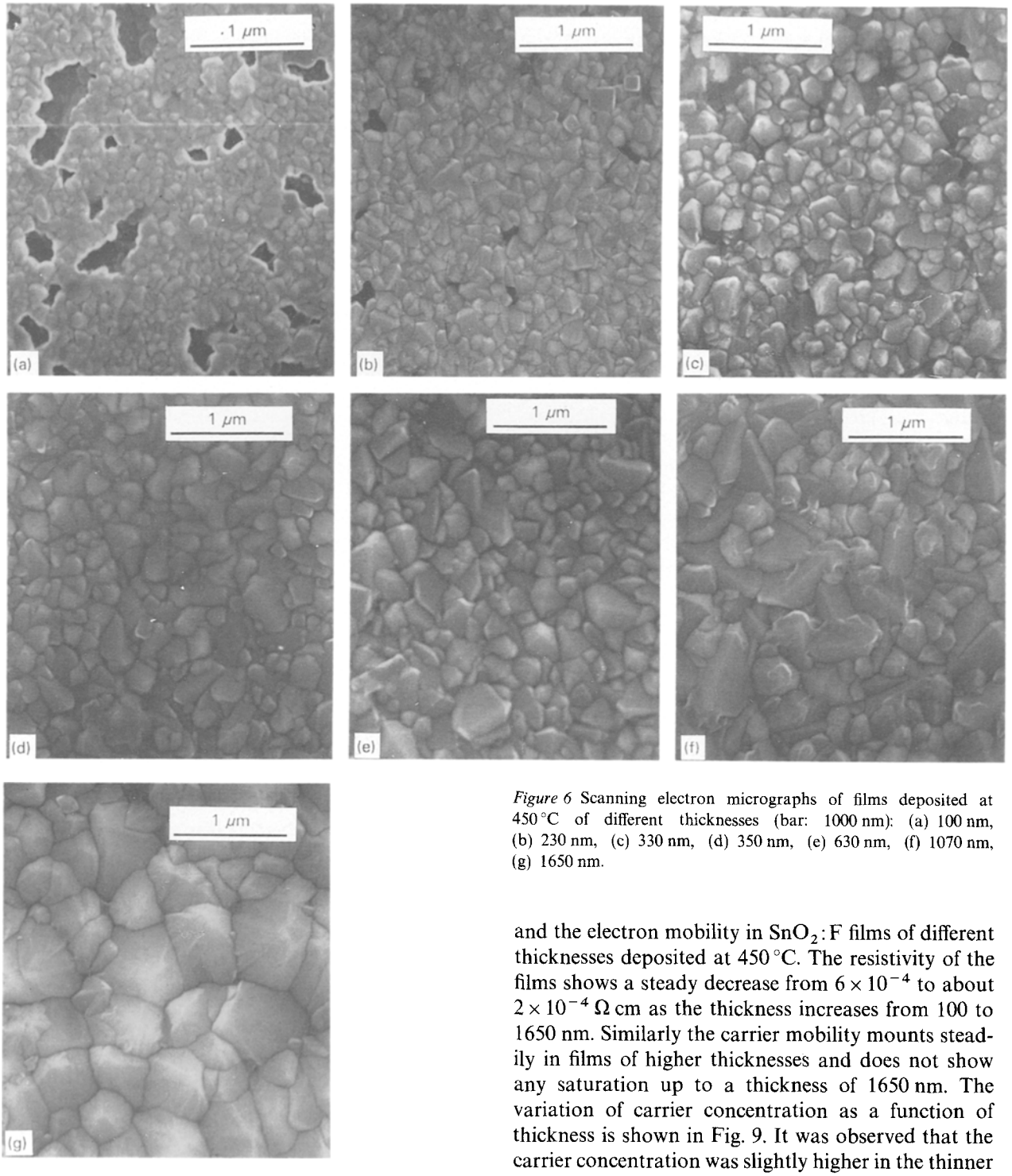

Figure 6 Scanning electron micrographs of films deposited at 450 °C of different thicknesses (bar: 1000 nm): (a) 100 nm, (b) 230 nm, (c) 330 nm, (d) 350 nm, (e) 630 nm, (f) 1070 nm, (g) 1650 nm.

0.65 nm s^{-1} at 510 °C (Fig. 3). The activation energy calculated from the Arrhenius plot of the deposition rate and the deposition temperature is about 10 kCal, which implies that the deposition process is thermally activated. This suggests that the deposition process is not limited by gas-phase diffusion but is controlled by surface reaction consisting of adsorption and desorption of the gas phase species [24] and it falls in the chemical vapour deposition regime. Similar observation of vapour phase growth in pyrosol process has been reported [25].

3.3. Variation of electrical properties

3.3.1. Effect of thickness

Fig. 8 shows the variation of the electrical resistivity and the electron mobility in SnO_2:F films of different thicknesses deposited at 450 °C. The resistivity of the films shows a steady decrease from 6×10^{-4} to about 2×10^{-4} Ω cm as the thickness increases from 100 to 1650 nm. Similarly the carrier mobility mounts steadily in films of higher thicknesses and does not show any saturation up to a thickness of 1650 nm. The variation of carrier concentration as a function of thickness is shown in Fig. 9. It was observed that the carrier concentration was slightly higher in the thinner films (< 200 nm thick) but did not vary significantly with increasing film thicknesses and was around 6×10^{20} cm^{-3}.

The higher mobility with increasing thicknesses of the SnO_2:F films deposited at 450 °C results from an increase in the grain size (and also the volume fraction of the crystallites) with thickness (Fig. 6). Similar variation of the mobility with thickness has been reported by several authors [26, 27]. The higher carrier concentration in the thinner films (< 200 nm thick) may arise from the presence of oxygen-rich surface layers as has also been observed by others [28, 29]. Thermodynamical calculations show that the atmosphere during deposition is oxidizing. This further justifies the view that oxygen-rich surface layers result in the higher carrier concentration observed in the thinner films.

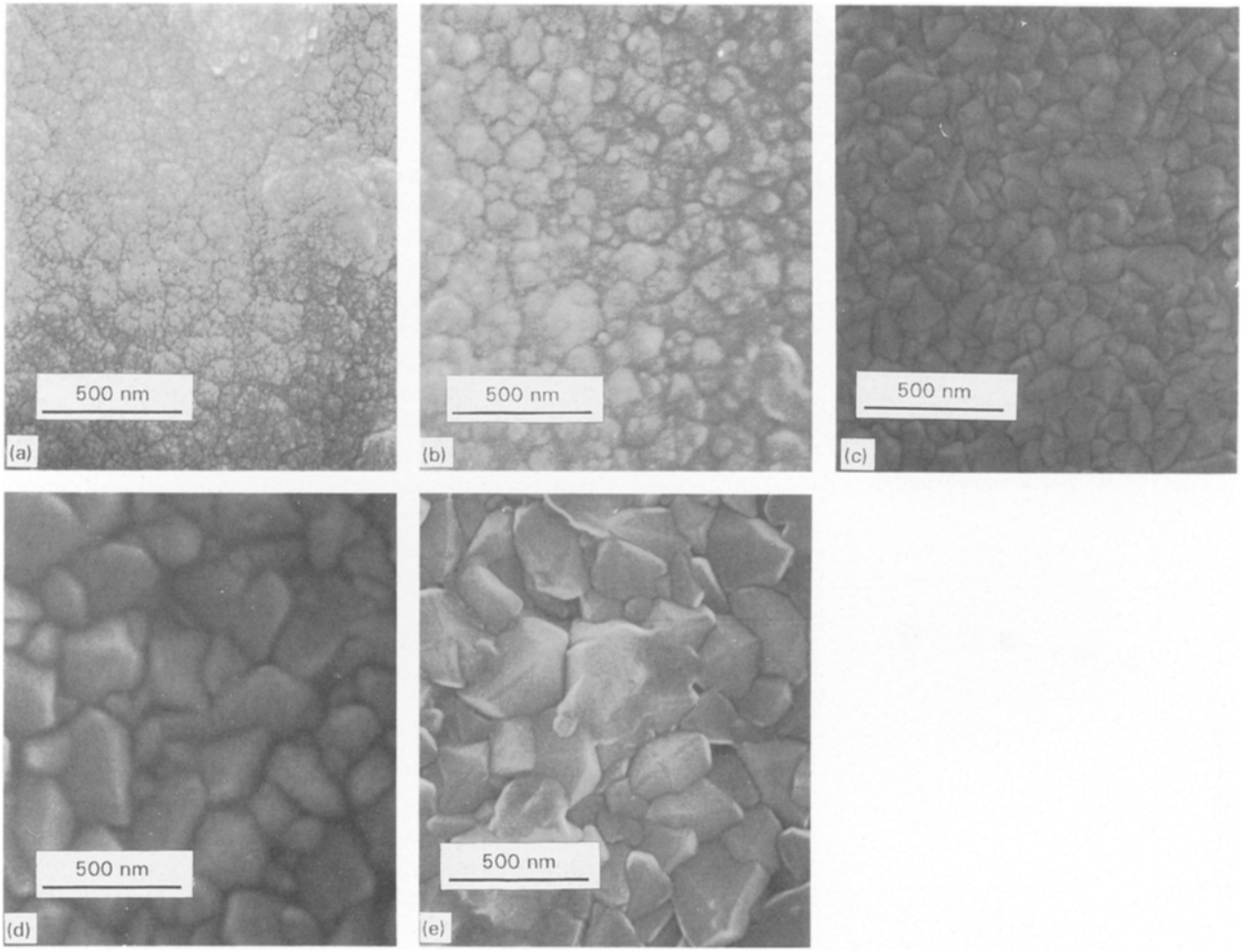

Figure 7 Scanning electron micrographs of films deposited at different substrate temperatures (bar: 500 nm): (a) 360 °C and 330 nm thick, (b) 380 °C and 400 nm thick, (c) 410 °C and 430 nm thick, (d) 450 °C and 630 nm thick, (e) 510 °C and 590 nm thick.

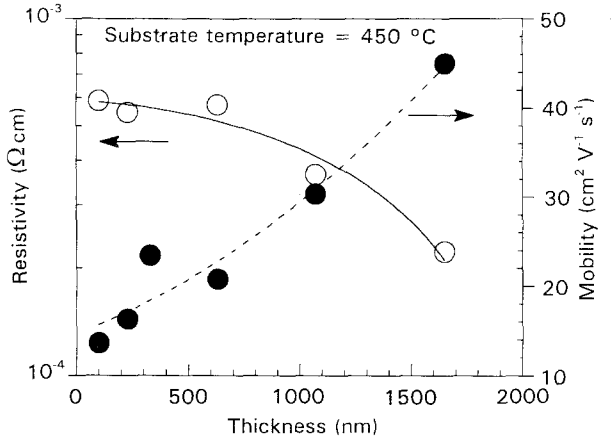

Figure 8 Resistivity and mobility versus thickness of films deposited at 450 °C.

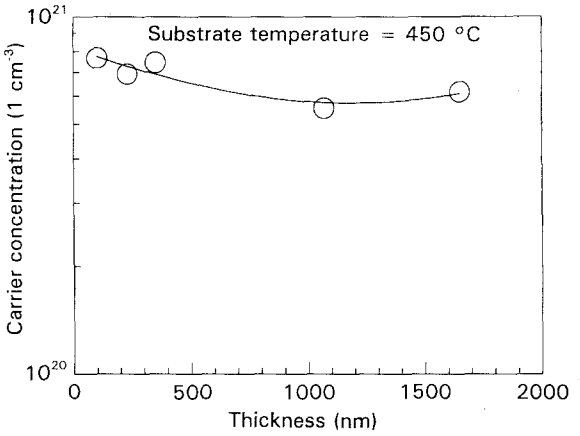

Figure 9 Carrier concentration versus thickness of films deposited at 450 °C.

3.3.2. Effect of substrate temperature

The variation of resistivity and mobility of SnO_2:F films deposited at varying substrate temperatures (thicknesses varying between 400 and 600 nm) is plotted in Fig. 10. Resistivity decreases from 2×10^{-3} Ω cm for films deposited at 360 °C to 6×10^{-4} Ω cm for films deposited at 450 °C, but then increases to 2×10^{-3} Ω cm for the films deposited at 510 °C. Mobility follows a reverse trend and reaches a maximum of ~ 21 cm^2 V^{-1}s^{-1} for samples deposited at 450 °C, but then decreases to about 18 cm^2 V^{-1}s^{-1} for the samples deposited at 510 °C, not really changing as sharply as the resistivity in the films deposited at temperatures higher than 450 °C.

Following similar arguments as presented in the previous section, the increase in crystal size distribution with increasing substrate temperature (Fig. 7) leads to an increase in carrier mobility and hence a

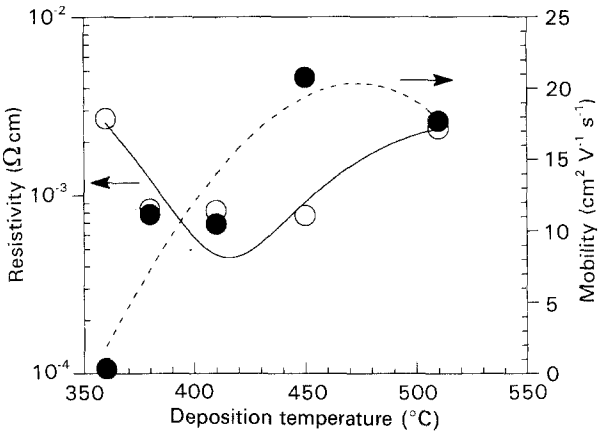

Figure 10 Variations of resistivity and mobility of films (330–600 nm thick) with deposition temperature.

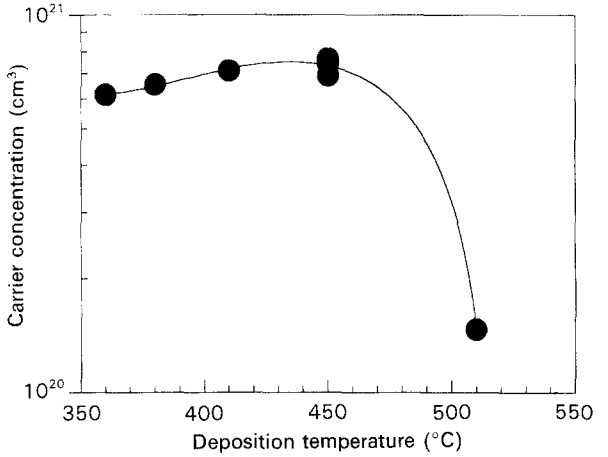

Figure 11 Variation of carrier concentration in films deposited at different temperatures.

decrease in the resistivity of the films deposited up to a substrate temperature of 450 °C, as the carrier concentration does not vary appreciably in these films (6×10^{20} cm^{-3}). However, for the films deposited at 510 °C the carrier concentration reduces dramatically (Fig. 11) leading to an increase in resistivity. This reduction in carrier concentration could be due to lower oxygen vacancies and/or lower active fluorine sites in the films [1]. The decrease in active vacancy sites can be reasoned to arise from the change in deposition mechanism. It may be noted here that the deposition rate increases rapidly from about 0.3 nm at 450 °C to 0.65 at 510 °C (Fig. 3). This increase in deposition rate, which is related to the increase in deposition temperature, suggests that the vapour pressures of the precursors are not completely thermally equilibrated [30]. In other words, the time for the precursors to equilibrate with respect to the substrate or, equivalently, to diffuse towards energetically favorable sites, decreases. The slight decrease in carrier mobility at 510 °C compared with those in the films deposited at 450 °C (Fig. 10) can be attributed to imperfect crystallization arising due to the higher deposition rates forbidding the growing SnO_2 lattice to relax to energetically favourable configuration, and hence resulting in the formation of defects. Such a phenomenon has been noticed in the deposition of other thin films like microcrystalline silicon films [31, 32].

3.4. Optical properties

The optical properties of SnO_2:F films are of utmost importance as these films are generally used as transparent electrodes in opto-electronic devices. However, since the surface morphology becomes rougher with increasing thickness and/or substrate temperature, it is essential to evaluate carefully the optical properties by taking the morphology into consideration. For transmittance measurements care has to be taken to differentiate between the specular and scattered components of the incident light. In some applications, as for example in the preparation of amorphous silicon solar cells, the surface morphology is profitably utilized to increase the light trapping efficiency in the solar cells [33, 34]. Using the procedure described above for transmittance measurements, the haze ratio can be defined as:

$$\text{Haze (\%)} = 100 \times \frac{(\text{MLT} - \text{specular transmittance})}{(\text{MLT})}$$

The haze ratio serves as a guide to distinguish between diffuse and specular transmittances and is a useful parameter for the evaluation of TCO substrates, especially for solar cell applications.

The variation of MLT and haze ratio of the SnO_2:F films deposited at 450 °C with respect to the thickness of the films is shown in Fig. 12. The MLT of the SnO_2:F films reported here is fairly constant (> 80%) for up to about 500 nm thick films but reduces steadily for thicker films. This is not at all surprising as the films attain an adequate crystalline structure for thicknesses ranging between 300 and 500 nm (as explained earlier) and hence the increased absorption by the crystallites is counterbalanced by the decrease in the number of grain boundaries, which otherwise absorb more light than the crystallites due to the higher level of defects in the grain boundary region. The steady rise in the haze ratio with increasing thickness of the films can be correlated to the increased surface roughness of the films.

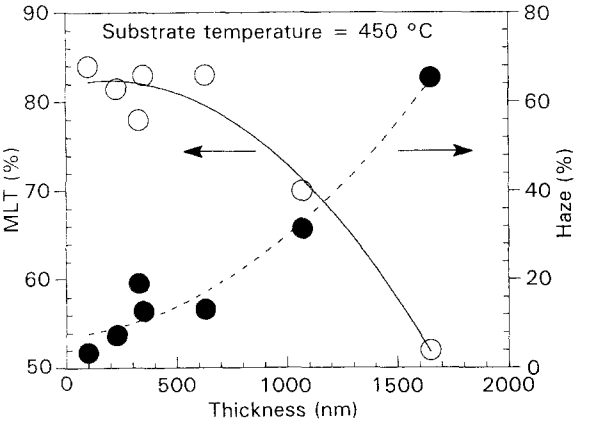

Figure 12 Variations of matching liquid transmittance and haze ratio with film thickness.

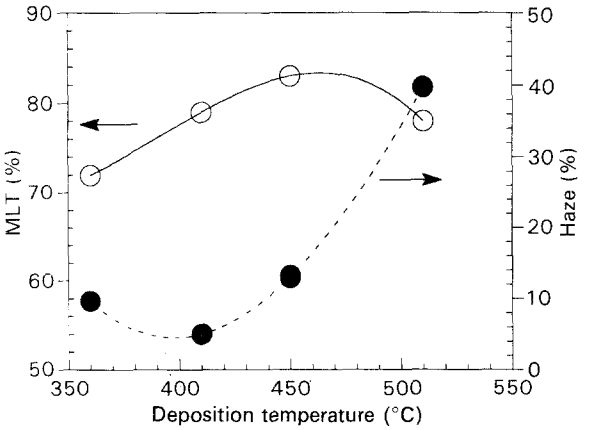

Figure 13 Variations of matching liquid transmittance and haze ratio with deposition temperature.

The variation of MLT and haze ratio with respect to the deposition temperature of the films is plotted in Fig. 13. The MLT of the films increases with increasing deposition temperature up to 450 °C. At higher deposition temperatures (510 °C) it decreases. The increase in the MLT of the films with increasing deposition temperature is also a direct consequence of the better crystalline structure attained in the films deposited at higher temperatures. The decrease in MLT for the film deposited at 510 °C is due to increased absorption in these films [13].

4. Conclusion

Pyrosol deposition is well suited for deposition of SnO_2:F films on glass as the deposition rates are high (0.1–0.65 nms^{-1}) and the technique is fairly simple. It is a two-stage process in which the precursors are produced in the aerosol followed by the CVD of the reactants. It has been demonstrated that the deposition from a solution in methanol actually starts from a $SnCl_4 \cdot 2CH_3OH$ complex. In order to know the chemical nature and the quantities of species during film deposition, the authors have developed an approach which consists of minimizing the enthalpy of the whole system. They have shown that (i) $SnCl_4$ is completely converted into solid SnO_2, (ii) the surrounding atmosphere during deposition is oxygen-rich, and (iii) chlorine, initially in the form of $SnCl_4$, transforms mainly into Cl_2 and HCl, which are believed to influence the growth of the crystallites and the surface morphology of the deposited films.

The growth pattern of thin SnO_2:F (< 350 nm) depositions was found to be heterogeneous and several thermal cracks were visible, possibly arising due to lattice mismatch. The volume fraction of crystallites does not change appreciably in films thicker than 350 nm. However, the crystallite size increases continuously up to 1650 nm thickness. The crystallinity in the films improved with the deposition temperature and films deposited above 410 °C develop crystallites. Films deposited at temperatures higher than 450 °C were found to develop crystallites of scattered sizes. This was correlated to the high deposition rates at such high temperatures which does not allow the species responsible for the film growth to diffuse over long distances over the growing film surface, hence decreasing the possibility of selecting energetically favourable sites. This has been argued to be the reason for the changes in mobility and resistivity observed in the films deposited at temperatures higher than 450 °C.

Detailed electrical and optical characterization of the deposited films was carried out. It was observed that the resistivity decreased and mobility increased with increasing film thickness due to the increase in grain size of the crystallites in the films. The majority carrier concentration was however practically unaffected by the increase in thickness (> 200 nm). The MLT of the films was constant up to a thickness of about 500 nm but decreased thereafter, which has been related to the increased absorption in the films. Optimized films around 600 nm thick had a resistivity of 6×10^{-4} Ω cm, a mobility of 20 $cm^2 V^{-1} s^{-1}$, a carrier concentration of 8×10^{20} cm^{-3} and an MLT of > 80%. These films are quite suitable for applications as transparent electrodes in opto-electronic devices and especially in solar cells.

Acknowledgements

The authors are thankful to Drs François Leblanc, Bernard Pateyron and Guy Delluc for making available some of their modelling results prior to publication, and to Mr Pierre Roubeau from Promophy in Palaiseau (France) for advice and technical support.

References

1. K. L. CHOPRA, S. MAJOR and D. K. PANDYA, *Thin Solid Films* **102** (1983) 1.
2. British Patent 632 (1942) 256.
3. G. BLANDENET, M. COURT and Y. LAGARDE, *Thin Solid Films* **77** (1981) 81.
4. H. IDA, T. MISHUKU, A. ITO, K. KATO, M. YAMANAKA and Y. HAYASHI, *Sol. Energy Mater.* **17** (1988) 407; *Trans. IEE Japan* **108-A** (1988) 543.
5. K. H. YOON and J. S. SONG, *Sol. Energy Mater. and Sol. Cells* **28** (1993) 28.
6. M. VALLET-REGI, V. RAGEL, J. ROMÀN, J. L. MARTINEZ, M. LABEAU and J. M. GONZÀLEZ-CALBET, *J. Mater. Res.* **8** (1993) 138.
7. K. SATO, Y. GOTOH, Y. HAYASHI, K. ADACHI and H. NISHIMURA, in "Tech. Digest of Int. PVSEC-5", edited by Y. Hamakawa (Kyoto, Japan, 1990) p. 1032.
8. R. G. GORDON, J. PROSCIA, F. B. ELLIS, Jr. and A. E. DELAHOY, *Sol. Energy Mater.* **18** (1989) 263.
9. H. NISHIMURA, *Business Japan* **9** (1990) 51.
10. G. HAACKE, *Ann. Rev. Mater. Sci.* **7** (1977) 73.
11. J. DUTTA, P. ROUBEAU, T. EMERAUD, J. M. LAURENT, A. SMITH, F. LEBLANC and J. PERRIN, *Thin Solid Films*, **239** (1994) 150.
12. D. W. KOON and C. J. KNICKERBOCKER, *Rev. Sci. Instrum.* **64** (1993) 510; D. W. Koon, *ibid.* **60** (1989) 271.
13. F. LEBLANC, Doctoral thesis, Université de Paris-sud, Centre d'Orsay (1992). Also Private communication.
14. Gmelin. In "Hanbuch der Anorganischen Chemie – Tin Part C5", (Springer Verlag, New York, 1977) p. 68.
15. "Handbook of Chemistry and Physics", 66th Edn, edited by R. C. Weast (CRC Press Inc., Boca Raton, FL, 1986) p. C-351.
16. *Ibid.* p. B-153.
17. G. DELLUC, B. PATEYRON and M. F. ELCHINGER, in "ADEP, Banque de Données de l'Université et du CNRS",

edited by Direction des Bibliothèques des Musées et de l'Information Scientifique et Technique (F. L. A. Consultants, Paris, 1986–1989).
18. W. B. WHITE, S. M. JOHNSON and B. DANTZIG, *J. Chem Phys.* **28** (1958) 751.
19. R. N. GHOSHTAGORE, *J. Electrochem. Soc.* **125** (1975) 110.
20. M. VERNON, T. R. HAYES and V. M. DONNELLY, *J. Vac. Sci. Technol.* **A10** (1992) 3499.
21. D. W. READEY, in "Ceramic Transaction–Sintering of Advanced Ceramics", edited by C. A. Handwerker (American Ceramic Society, Cincinatti, OH, USA, 1988) p. 86.
22. N. KRISTENSEN, F. ERICSON, J. A. SCHWEITZ and U. SMITH, *Thin Solid Films* **197** (1991) 67.
23. R. RODRIGUEZ-CLEMENTE, A. FIGUERAS, S. GARELIK, B. ARMAS and C. COMBESARE, *J. Cryst. Growth* **125** (1992) 533.
24 C. E. MORASANU, in "Thin Film Science and Technology", Vol. 7, edited by G. Siddall (Elsevier, Amsterdam, 1990) p. 104.
25. W. M. SEARS and M. A. GEE, *Thin Solid Films* **165** (1988) 265.
26. H. DE WAAL and F. SIMONIS, *ibid.* **77** (1981) 253.
27. M. BUCHANAM, J. B. WEBB and D. F. WILLIAMS, *ibid.* **80** (1981) 373.
28. J. L. VOSSEN, *RCA Rev.* **32** (1971) 269.
29. H. HOFFMANN, A. DIETRICH, J. PICKL and D. KRAUSE, *Appl. Phys.* **16** (1978) 381.
30. K. L. CHOPRA, in "Thin Film Phenomena", edited by K. L. Chopra (McGraw-Hill, New York, 1969) p. 138.
31. J. DUTTA, A. L. UNAOGU, S. RAY and A. K. BARUA, *J. Appl. Phys.* **66** (1989) 4709.
32. K. TANAKA and A. MATSUDA, *Mater. Sci. Rep.* **2** (1987) 139.
33. J. MORRIS, R. R. ARYA, J. G. O'DOWD and S. WIEDEMAN, *J. Appl. Phys.* **67** (1990) 1079.
34. A. CATALANO, in "Amorphous and Microcrystalline Devices: Opto-electronic Devices", edited by Jerzy Kanicki (Artech House, Boston, 1991) p. 9.

Received 31 January
and accepted 27 May 1994